Enthalpy relaxation and annealing effect in polystyrene

Waki Sakatsuji,* Takashi Konishi, and Yoshihisa Miyamoto
Graduate School of Human and Environmental Studies, Kyoto University, Yoshida-nihonmatsu-cho, Sakyo-ku, Kyoto 606-8501, Japan
(Received 4 March 2013; published 23 July 2013)

The effects of thermal history on the enthalpy relaxation in polystyrene are studied by differential scanning calorimetry. The temperature dependence of the specific heat in the liquid and the glassy states, that of relaxation time, and the exponent of the Kohlrausch-Williams-Watts function are determined by measurements of the thermal response against sinusoidal temperature variation. A phenomenological model equation previously proposed to interpret the memory effect in the frozen state is applied to the enthalpy relaxation and the evolution of entropy under a given thermal history is calculated. The annealing below the glass transition temperature produces two effects on enthalpy relaxation: the decay of excess entropy with annealing time in the early stage of annealing and the increase in relaxation time due to physical aging in the later stage. The crossover of these effects is reflected in the variation of temperature of the maximum specific heat observed in the heating process after annealing and cooling.

DOI: 10.1103/PhysRevE.88.012605 PACS number(s): 61.25.H−, 61.20.Lc, 61.43.Fs, 64.70.pj

I. INTRODUCTION

The glass transition is a freezing phenomenon from the liquid state to the glassy state with lowering temperature and occurs when the characteristic time of the system becomes longer than the experimental time scale. Near and below the glass transition temperature T_g, the thermodynamic variables, e.g., volume, enthalpy, and entropy, relax toward the equilibrium values and the relaxation process is known to be nonlinear and slower than the single exponential decay [1–3]. Nonlinearity is a feature in structural relaxation in the sense that the structural relaxation time depends not only on temperature but also on the instantaneous out-of-equilibrium structure of the system [2]. Since the time course of the control parameters in the freezing process is memorized in the glassy state [4], the instantaneous relaxation time depends on the thermal history from the equilibrium state up to the instantaneous out-of-equilibrium state. In this study, we discuss the dynamics of relaxation time under a given thermal history in enthalpy relaxation.

A characteristic of enthalpy relaxation is typically the overshoot in the specific heat in the glass transition range in the heating process after cooling to a temperature well below T_g, which depends on the cooling and heating rates, and the isothermal annealing conditions [3,5–8]. Illuminative diagrams are given by Moynihan *et al*. to qualitatively explain the enthalpy relaxation [5]. Enthalpy relaxation has been analyzed using phenomenological models, e.g., the Tool-Narayanaswamy-Moynihan (TNM) model [6–8], Kovacs-Aklonis-Hutchinson-Ramos model [9] and Gómez-Monleón model [10]. In the most widely employed TNM model, the evolution of fictive temperature T_f, introduced by Tool [6], is expressed by a model equation. In this model the relaxation time is assumed to depend on both the actual temperature T and the fictive temperature and a nonlinearity parameter x is introduced to partition the activation energy into T and T_f. The Gómez-Monleón model describes the evolution of configurational entropy by extending the relation between the relaxation time and the configurational entropy given by Adam and Gibbs [11] to the out-of-equilibrium states and introduces the entropy of the limit state S_c^{lim} attained after an infinitely long annealing time that is different from the extrapolation of entropy from temperature higher than T_g. These models have been reported to satisfactorily reproduce the experimental results after a given thermal history [12–19]. In these models, however, in addition to the nonlinearity parameter x, the parameters connecting the relaxation time to T_f or S_c^{lim} and the exponent β of the Kohlrausch-Williams-Watts (KWW) function [20] are parameters to be determined by the fitting to the experimental results. It is therefore difficult to examine the physical significance of the obtained parameters [2].

We have proposed a phenomenological model equation as a natural extension of the linear rheology in order to study the memory effect in the frozen state [4]. The phenomenological model equation can be straightforwardly applied to the enthalpy relaxation to give the enthalpy $H(t)$ and entropy $S(t)$ against a given thermal history $T(t';t'<t)$ and the resulting formula is equivalent to the Gómez-Monleón model when it is transformed by formal integration by parts. In this study we discuss how the model equation with parameters experimentally determined explains the out-of-equilibrium behavior of the enthalpy rather than discuss whether the present model can reproduce the experimental specific heat more quantitatively than the models hitherto proposed [5–10]. We have studied the enthalpy relaxation of polymethylmethacrylate by differential scanning calorimetry (DSC) and shown that the model equation reproduces two peaks in specific heat observed in the heating process after annealing at a low temperature [21].

The purpose of the present study is to clarify the features of annealing effects in enthalpy relaxation, in particular the time and temperature dependence of the relaxation time, based on the experimental results and the analysis by the model calculations. In order to reduce the number of parameters employed in the calculation, we will experimentally determine the basic relaxation parameters. A typical amorphous polymer, atactic polystyrene, is used as a material. First we measure the frequency and temperature dependence of complex specific heat from the response of heat flow against the sinusoidal temperature variation. These measurements determine the

*sakatsuji.waki.87s@st.kyoto-u.ac.jp

temperature dependence of specific heat in the liquid and the glassy states and that of the relaxation time. The exponent β of the KWW function is estimated from the normalized complex specific heat. Then we measure the specific heat in the heating process after various thermal histories and compare the results of the calculation by the proposed model equation with the experimental results. After discussing the calculation with only the thermal relaxation parameters experimentally determined, we take account of the additional contribution to the glassy configurational entropy due to the temperature dependence of the free energy landscape (FEL) based on the FEL theory [22–24] for quantitative examination.

II. EXPERIMENT

A. Material and differential scanning calorimetry

The material used in this study was atactic polystyrene (aPS) with a molecular weight $M_w = 280\,000$ purchased from Scientific Polymer Products. The DSC measurement was carried out using a DSC-60 (Shimadzu Corporation) under nitrogen gas atmosphere. Ethanol cooled at $-25\,^\circ$C was circulated in the cooling block in order to obtain cooling rates up to 70 K/min. The temperature calibration was made by the melting point of indium. The measurements described below were performed on polystyrene, alumina, and a vacant pan under the same condition and the values of heat flux were calibrated. The specific heat C_p is defined by $C_p = \dot{Q}/w\dot{T}$, where $\dot{Q}$ is the heat flux observed in the measurement, w is the weight of the sample, and $\dot{T}$ is the time derivative of temperature T. In all the experiments, the memories of the samples were erased by annealing at 200 °C for 1 min.

B. Complex specific heat measurements

A sample of about 4 mg and 0.2 mm in thickness was cooled to a temperature T_0 in the range from 40 °C to 160 °C at 9.5 K/min and kept for 3 min. Then the sample underwent a sinusoidal temperature variation centered at T_0 with an amplitude of 0.5 K and a period P in the range from 20 to 200 s.

Fourier coefficients with period P were calculated from the heat flux in the steady state to give the absolute value $|C_p^*(\omega,T)|$ and the phase difference caused by the relaxation process $\delta_{relax}(\omega,T)$ of the complex specific heat $C_p^*(\omega,T)$, where ω is the angular frequency given by $2\pi/P$. Since phase difference obtained from the measurement showed finite values outside the glass transition region due to the effects of the heat transfer, δ_{relax} was determined by assuming that δ_{relax} well above and below T_g is zero [25]. The real part C_p' and the imaginary part C_p'' of specific heat are given by $C_p^* = C_p' - iC_p'' = |C_p|e^{i\delta_{relax}}$ ($i = \sqrt{-1}$).

C. Rate cooling and annealing

In the measurements of the dependence of enthalpy relaxation on the cooling rate and the annealing condition, samples of 4–13 mg were employed; no systematic variation in the heat flow with the sample weight was observed. The sample was cooled from 200 °C to 30 °C at a rate of $\dot{T}_c$ in the range from 0.1 to 30 K/min and heated to 200 °C at 9.5 K/min followed by the second run. The second run comprises the cooling from 200 °C to 30 °C at 9.5 K/min and heating to 180 °C at 9.5 K/min, the results of which are used for the baseline correction and the examination of the sample degradation.

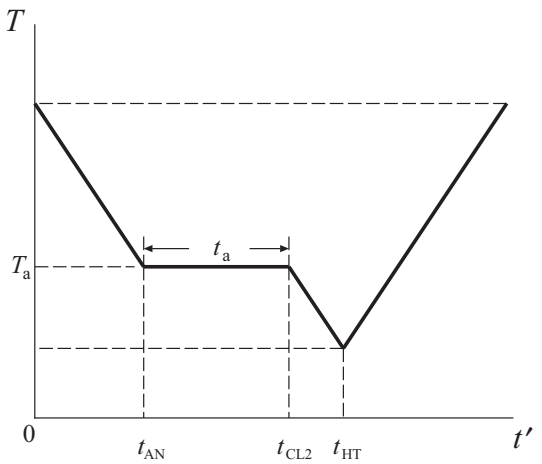

FIG. 1. Schematic diagram of the thermal history in the annealing measurement.

Figure 1 shows the thermal history of the annealing measurement. In the annealing experiments, the sample was cooled from 200 °C to an annealing temperature T_a in the range from 60 °C to 110 °C at 9.5 K/min, annealed for t_a in the range from 1 to 10^4 min, further cooled to 30 °C, and then heated to 200 °C at 9.5 K/min followed by the second run as above. All the thermal treatments were carried out in the calorimeter.

III. PHENOMENOLOGICAL MODEL AND CALCULATION OF SPECIFIC HEAT

The phenomenological model equation applied to the entropy $S(t)$ at time t is given as a functional of the thermal history $T(t';t' < t)$ [4] by

$$S(t) = S^{eq}[T(t)] - \int_{-\infty}^{t} \overline{\Delta\chi}[T(t),T(t')][T(t) - T(t')] \times \frac{\partial\phi[\tilde{t}(t,t')]}{\partial t'}dt', \quad (1)$$

where $S^{eq}(T)$ is the entropy in the equilibrium liquid state and $\overline{\Delta\chi}[T(t),T(t')]$ is the susceptibility for entropy given by

$$\overline{\Delta\chi}[T(t),T(t')] = \frac{1}{T(t) - T(t')}\int_{T(t')}^{T(t)} \frac{\Delta C_p(T'')}{T''}dT'', \quad (2)$$

where $\Delta C_p(T)$ is the difference between the liquid and the glassy specific heat $C_p^0(T)$ and $C_p^\infty(T)$, respectively, and $\phi(t)$ is the normalized relaxation function. The intrinsic time lapse, or the reduced time $\tilde{t}(t,t)$ is defined by

$$\tilde{t}(t,t') \equiv \int_{t'}^{t} \frac{du}{\tau(u)}, \quad (3)$$

which gives the time lapse between t' and t measured with the instantaneous relaxation time $\tau(u)$.

The relaxation time is assumed to obey the Adam-Gibbs theory in the out-of-equilibrium glassy state as well as in the

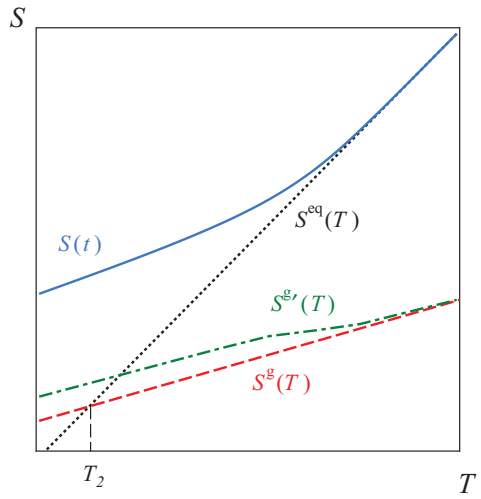

FIG. 2. (Color online) Schematic graph of entropy vs temperature. The solid, dotted, dashed, and dash-dotted lines represent the instantaneous entropy $S(t)$, the liquid entropy $S^{eq}(T)$, the hypothetical glassy entropy $S^{g}(T)$ defined by Eq. (6), and the modified glassy entropy $S^{g\prime}(T)$ defined by Eq. (14), respectively. At a temperature T_2, S^{g} is equal to S^{eq}.

equilibrium liquid state [26,27] and is determined by

$$\tau = \tau_\infty \exp\left[\frac{A}{TS_c}\right], \tag{4}$$

where τ_∞ and A are constants. The configurational entropy S_c is given by

$$S_c = S - S^g(T), \tag{5}$$

where $S^g(T)$ is the hypothetical glassy entropy defined by

$$S^g(T) = S^{eq}(T_2) + \int_{T_2}^{T} \frac{C_p^\infty(T')}{T'}\, dT', \tag{6}$$

which is equal to the entropy of the equilibrium liquid $S^{eq}(T)$ at T_2 as schematically shown in Fig. 2. The entropy S in Eq. (5) is defined later depending on the calculation methods. Equation (1) with Eq. (5) is basically equivalent to the models proposed for the analysis of enthalpy relaxation [10,14,26].

IV. RESULTS AND DISCUSSION

A. Relaxation parameters

Figure 3 shows the temperature dependence of the real and imaginary parts of specific heat for the period from 20 to 200 s. The real part of specific heat $C_p'(T)$ gives the specific heat in the liquid state $C_p^0(T)$ at high temperatures and that in the glassy state $C_p^\infty(T)$ at low temperatures. Assuming that both $C_p^0(T)$ and $C_p^\infty(T)$ are linear in T in the range of the measurement, i.e., $C_p^0(T) = a^\ell T + b^\ell$ and $C_p^\infty(T) = a^g T + b^g$, the coefficients of C_p^0 and C_p^∞ are obtained from the high- and low-temperature data for all periods: $a^\ell = 3.7 \times 10^{-3}$ J g^{-1} K^{-2}, $b^\ell = 6.1 \times 10^{-1}$ J g^{-1} K^{-1}, $a^g = 4.1 \times 10^{-3}$ J g^{-1} K^{-2}, and $b^g = 9.0 \times 10^{-2}$ J g^{-1} K^{-1}. Although there is a small difference between our results and the ones in the literatures [28–30] as shown in Fig. 3 by the solid symbols, this difference is not critical to the

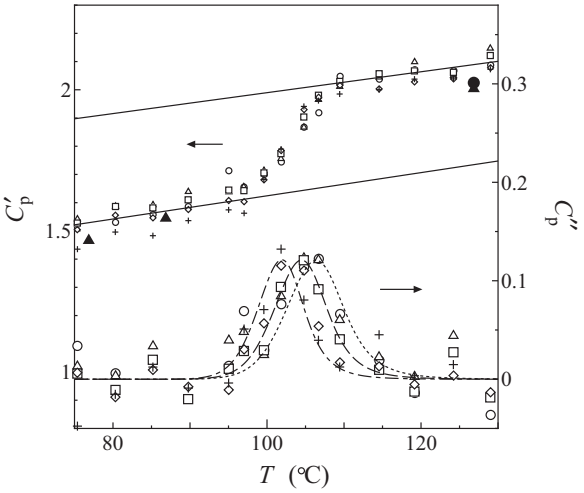

FIG. 3. Temperature dependence of the real (upper data) and imaginary (lower data) parts of the specific heat. The symbols represent the experimental data: ○, $P = 20$ s; △, $P = 30$ s; □, $P = 50$ s; ◇, $P = 100$ s; and +, $P = 200$ s. The solid lines represent C_p^0 (upper) and C_p^∞ (lower), respectively. The dotted, dashed, and dash-dotted lines represent C_p'' calculated for $P = 20$, 50, and 100 s, respectively. The closed circle and triangles are the data from Refs. [28,29] by DSC, respectively.

discussion about the effects of annealing on the peak height and peak temperature and hence we adopt these values of a^ℓ, b^ℓ, a^g, and b^g.

Figure 4 shows the temperature dependence of relaxation time τ. Five of six data points shown by the circles in Fig. 4 are determined from a peak temperature T_α of C_p'' in Fig. 3 by $\tau(T_\alpha) = P/2\pi$ and one data point by $\tau(T) = 1/\omega_{max}$, where ω_{max} is the angular frequency at which $C_p''(\omega)$ shows a maximum at $T = 104.8$ °C. The relaxation times thus obtained

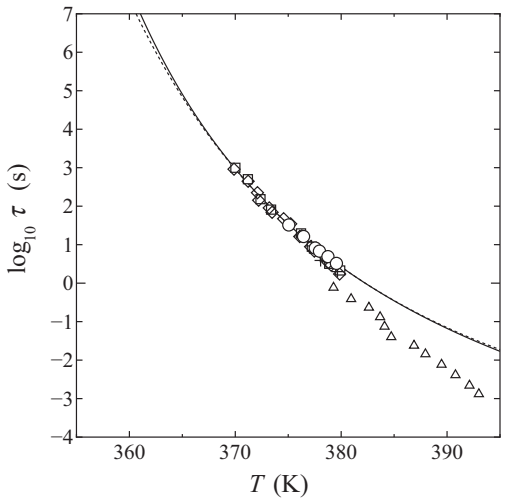

FIG. 4. Temperature dependence of relaxation time. Symbols represent the experimental results: ○, the results in the present study; □, TMDSC data [30]; ◇, TMDSC data [31]; +, TMDSC data [32]; and △, 3ω method [30]. The solid and dotted lines represent Eq. (4) with $\tau_\infty = 1.20 \times 10^{-8}$ s, $A = 333$ J g^{-1}, and $T_2 = 336$ K and the dotted line represents Eq. (4) with $\tau_\infty^{(3)} = 4.35 \times 10^{-9}$ s, $A^{(3)} = 550$ J g^{-1}, and $T_2^{(3)} = 329$ K, respectively.

are those in the equilibrium state and can be expressed by the Adam-Gibbs equation with $S_c(T) = S^{eq}(T) - S^g(T) = \int_{T_2}^{T} \frac{\Delta C_p(T')}{T'} dT'$. The least-squares fitting to our experimental results by Eq. (4) gives $\tau_\infty = 1.20 \times 10^{-8}$ s, $A = 333$ J g^{-1}, and $T_2 = 336$ K (the solid line in Fig. 4). The squares, rhombuses, and pluses in Fig. 4 are the data obtained by temperature-modulated DSC (TMDSC) [30–32] and triangles by the 3ω method [30]. The relaxation times by TMDSC agree with our results within the experimental accuracy. The literature data by the 3ω method in Fig. 4 are not used in the least-squares fitting because when they are included in the fitting, the maximum of the imaginary part of the normalized specific heat to be discussed below showed a broader half-width at lower frequencies than at higher frequencies, which is empirically considered not to be the case.

The normalized relaxation function $\phi(t)$ may be approximated by the stretched exponential function or the KWW function with an exponent β:

$$\phi\left(\frac{t}{\tau_{KWW}}\right) = \exp\left[-\left(\frac{t}{\tau_{KWW}}\right)^{\beta}\right], \tag{7}$$

where τ_{KWW} is the KWW relaxation time proportional to $\tau(T)$ and $\phi(t)$ gives the complex specific heat through the Fourier transform. The complex specific heat in Fig. 3 normalized by $\Delta C_p(T)$ and $\tau(T)$,

$$C_p^{N*}(\omega\tau) = \frac{C_p^*[\omega\tau(T)] - C_p^\infty(T)}{\Delta C_p(T)}, \tag{8}$$

is shown in Fig. 5. The normalized complex specific heat is calculated from the Fourier transform of $1 - \phi(t/\tau_{KWW})$ and compared with $C_p^{N*}(\omega\tau)$ in Fig. 5 in the range of $\omega\tau$ from 10^{-2} to 10^2. The normalized complex specific heat C_p^{N*} is satisfactorily reproduced by Eq. (7) as shown in Fig. 5 by the solid line: The best-fit values are $\beta = 0.62 \pm 0.09$ and $\tau_{KWW} = (0.79 \pm 0.19)\tau$. The relaxation times and the relaxation function thus obtained are those for the enthalpy.

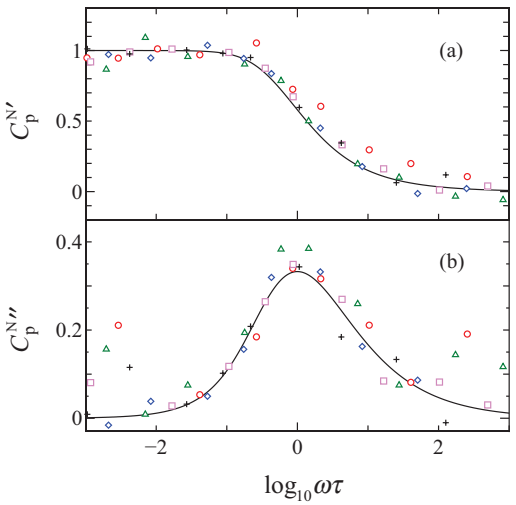

FIG. 5. (Color online) (a) Real and (b) imaginary parts of the normalized specific heat: ○, $P = 20$ s; △, $P = 30$ s; □, $P = 50$ s; ◇, $P = 100$ s; and +, $P = 200$ s. The solid curves represent the specific heats calculated from the Fourier transform of $1 - \phi(t/\tau_{KWW})$.

The entropic relaxation times determined by the maximum temperature or frequency of C_p''/T are indistinguishable from the enthalpic relaxation times in the present experimental accuracy. In the following discussion, therefore, we will assume that the relaxation times and the relaxation function are the same for enthalpy and entropy.

B. Dependence of specific heat on cooling rate and annealing conditions

Figure 6 shows the temperature dependence of specific heat on heating at 9.5 K/min after cooling at $\dot{T}_c$ in the range from 0.1 to 30 K/min. The magnitude of the maximum in specific heat $C_{p\,max}$ increases while the temperature of the maximum specific heat T_{max} decreases and then increases with decreasing $\dot{T}_c$. The glass transition temperature T_g defined by the equal area method [8], equivalent to the fictive temperature well below the glass transition range T_f' at 50 °C in this study, is 97.7 °C at the cooling rate of 9.5 K/min. One of the quantities characterizing the glassy state is the entropy deviation from the equilibrium value at $T_{low} = 50\,°C \ll T_g$, $\delta S(T_{low}) = S(T_{low}) -$

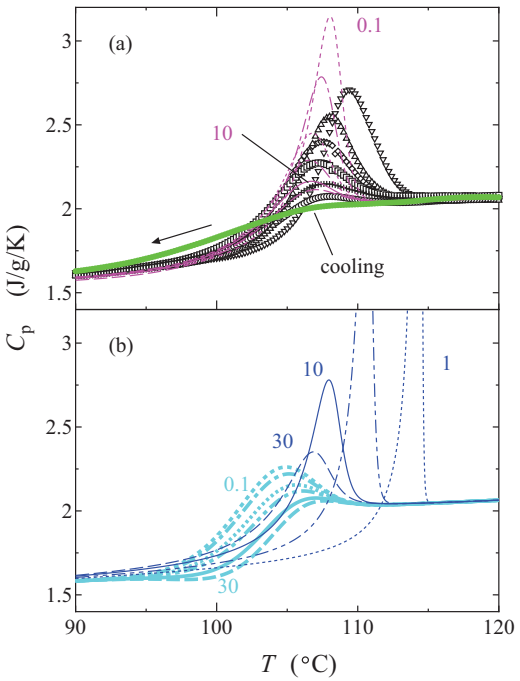

FIG. 6. (Color online) Specific heat vs temperature in the heating process after cooling at a constant rate. (a) Results of the cooling experiment and calculation 3 with $\Delta\chi_F = -6.17 \times 10^{-4}$ J g^{-1} K^{-2}, $\sigma_F = 23$ K, and $T_F = 371$ K. The specific heat in the cooling process for the cooling rate of 9.5 K/min are shown by circles [light green (light gray), experimental results]. (b) Calculations 1 [cyan (light gray), thick] and 2 [blue (dark gray), thin]. The symbols represent the experimental data: ▽, $\dot{T}_c = 0.1$; △, $\dot{T}_c = 0.3$; ◇, $\dot{T}_c = 1$; □, $\dot{T}_c = 3$; +, $\dot{T}_c = 10$; and ○, $\dot{T}_c = 30$ K/min. The short-dashed, dash-dotted, dotted, dash–double-dotted, solid, and dashed lines are the data for $\dot{T}_c = 0.1$, 0.3, 1, 3, 10, and 30 K/min, respectively. The results of calculation 2 for $\dot{T}_c = 0.3$ and 0.1 K/min are not shown in the figure because their T_{max} are beyond the range of this figure. The numbers in the figure represent the cooling rate before heating.

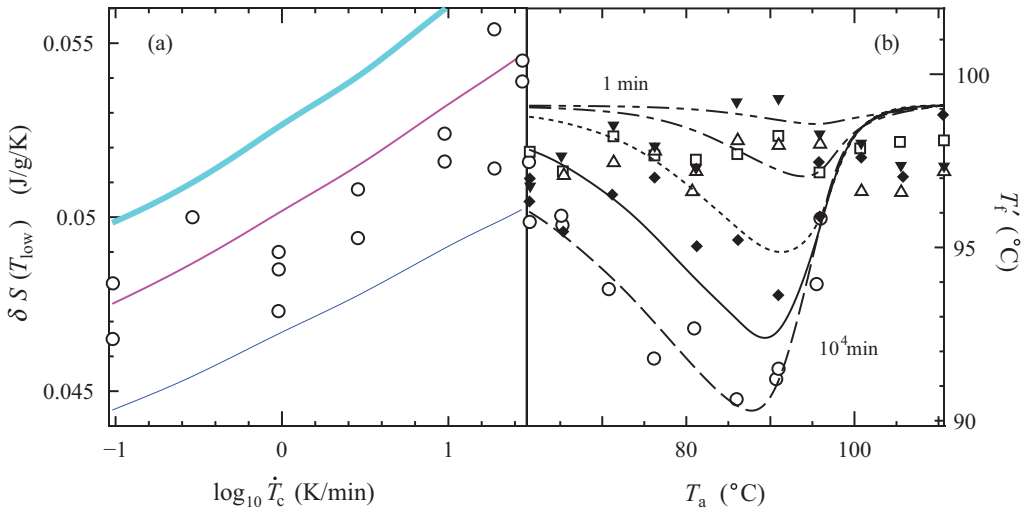

FIG. 7. (Color online) (a) Cooling rate dependence of $\delta S(T_{low})$. The symbols represent the results of cooling experiments and the curves the calculated ones. The top, middle, and bottom lines represent the results from calculations 1, 2, and 3, respectively. The line colors and thickness are the same as in Fig. 6. (b) Annealing temperature dependence of $\delta S(T_{low})$ for t_a from 1 to 10^4 min. The left axis T_f' is approximately proportional to $\delta S(T_{low})$. The symbols represent the experimental results: △, $t_a = 1$; ▼, $t_a = 10$; □, $t_a = 10^2$; ♦, $t_a = 10^3$; and ○, $t_a = 10^4$ min. The dash–double-dotted, dash-dotted, dotted, solid, and dashed lines are the results from calculation 3 for $t_a = 1$, 10, 10^2, 10^3, and 10^4 min, respectively.

$S^{eq}(T_{low})$, and shown in Fig. 7(a); $\delta S(T_{low})$ is approximately proportional to T_f' and decreases with decreasing $\dot{T}_c$.

The symbols in Figs. 8(a) and 9(a) show the annealing time dependence of the specific heat on heating at 9.5 K/min after annealing at 95.8 °C and 86.1 °C for t_a from 1 to 10^4 min. The results for $t_a = 10^4$ min are almost identical to the results for $t_a = 10^3$ min at $T_a = 95.8$ °C. Figures 8 and 9 show that C_{pmax} increases with annealing time t_a, while T_{max} decreases at $t_a < 10$ min and then increases with t_a. Figures 6, 8, and 9 indicate that $C_{p\,max}$ monotonically increases and T_{max} first decreases and then increases as the aging effects increase in aPS. The variations in T_{max} with cooling rate and annealing time are similar to those reported on the glassy polymers [10,19,33–35].

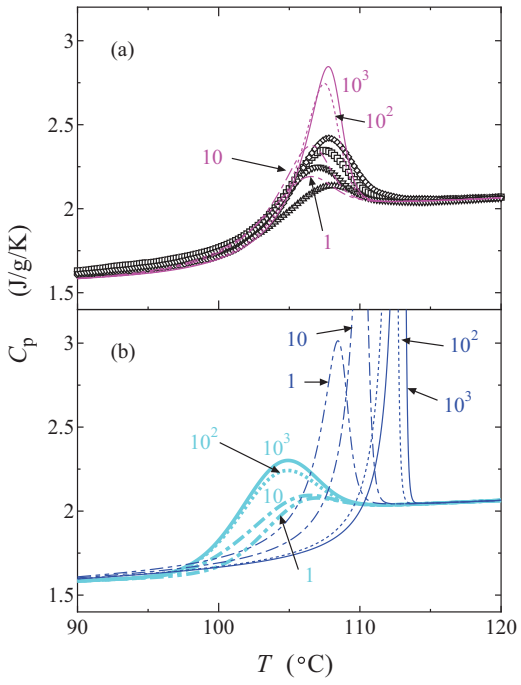

FIG. 8. (Color online) Specific heat on heating after annealing at $T_a = 95.8$ °C for t_a in the range from 1 to 10^3 min. (a) Results of the annealing experiments and those of calculation 3. (b) Calculations 1 and 2. The symbols show the experimental results: △, $t_a = 1$; ▽, $t_a = 10$; □, $t_a = 10^2$; and ◇, $t_a = 10^3$. The curves represent the results of calculations 1 [cyan (light gray), thick], 2 [blue (dark gray), thin] and 3. The line types are the same as in Fig. 7(b). The numbers in the figure represent the annealing time.

Figure 7(b) shows the dependence of $\delta S(T_{low})$ on annealing temperature and time. For $T_a > 100$ °C, i.e., $T_a > T_g$, $\delta S(T_{low})$ for all t_a are similar values while $\delta S(T_{low})$ decreases with annealing time t_a for $T_a \leqslant 90$ °C. Figure 10 shows the annealing time and temperature dependence of $C_{p\,max}$ and T_{max}. The specific heat maximum C_{pmax} remains almost unchanged at $T_a \geqslant 100$ °C and increases with t_a at $T_a < 100$ °C. The rate of increase in $C_{p\,max}$ is the largest at $T_a \approx 85$ °C. The temperature of the maximum specific heat T_{max} remains almost unchanged at $T_a \geqslant 100$ °C, it first decreases and increases with t_a at $70 \leqslant T_a < 100$ °C, and it decreases with t_a at $T_a < 70$ °C. At $95 \leqslant T_a \leqslant 100$ °C, $C_{p\,max}$ and T_{max} approach asymptotic values at long t_a, which suggests that the entropy reaches an equilibrium value within $t_a = 10^4$ min at $T_a \geqslant 95$ °C [36]. The annealing time at which T_{max} shows a minimum $t_{a\,min}(T_a)$ at a given T_a increases with decreasing T_a as shown by the arrows for $T_a = 95.8$ °C, 86.1 °C, and 76.2 °C in Fig. 10(b), though the scatter of data prevents us from precise determination of $t_{a\,min}(T_a)$. We expect from Fig. 10(b) that T_{max} decreases at short annealing time t_a, then increases, and approaches an asymptotic value for $t_a \to \infty$.

The experimental results for the enthalpy relaxation in aPS are summarized as follows.

(i) The deviation of entropy from the equilibrium value at $T_{low} = 50$ °C, $\delta S(T_{low})$, decreases with decreasing cooling rate $\dot{T}_c$ and with increasing annealing time t_a.

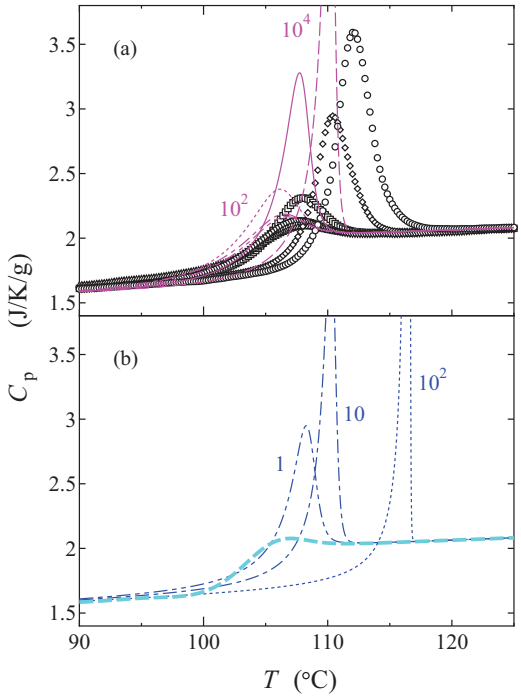

FIG. 9. (Color online) Specific heat on heating after annealing at $T_a = 86.1\,^\circ$C for t_a in the range from 1 to 10^4 min. (a) Results of the annealing experiments and those of calculation 3. (b) Results of calculations 1 and 2. The symbols show the experimental results: △, $t_a = 1$; ▽, $t_a = 10$; □, $t_a = 10^2$; ◇, $t_a = 10^3$; and ○, 10^4 min. The curves represent the results of calculations 1 [cyan (light gray), thick], 2 [blue (dark gray), thin] and 3. The line types are the same as in Fig. 7(b). The results from calculation 1 are almost identical to each other within $1 \leqslant t_a \leqslant 10^4$ min. The maximum of C_p from calculation 2 for $t_a = 10^4$ min is not included in this figure. The numbers in the figure represent the annealing time.

(ii) The maximum of specific heat in the heating process $C_{p\,max}$ decreases with T_c and increases with t_a at $T_a < 100\,^\circ$C. It approaches an asymptotic value with t_a at $95 \leqslant T_a \leqslant 100\,^\circ$C.

(iii) The temperature of maximum specific heat T_{max} first decreases with increasing t_a, then increases after passing a minimum at $t_{a\,min}(T_a)$ ($T_a < 100\,^\circ$C), and approaches an asymptotic value ($95 \leqslant T_a \leqslant 100\,^\circ$C). The variation of T_{max} with decreasing T_c qualitatively corresponds to that with increasing t_a.

C. Calculation by phenomenological model equation

The specific heat under a given thermal history is calculated with the relaxation parameters experimentally obtained for aPS in the following three methods according to the definition of configurational entropy S_c.

Calculation 1. The configurational entropy is assumed to be given by $S_c(T) = S^{eq}(T) - S^g(T)$. Hence the relaxation time is an equilibrium one and determined by the instantaneous temperature as in Fig. 4, i.e., $\tau(T) = \tau^{eq}(T)$.

Calculation 2. The configurational entropy at time t is assumed to be given by $S_c(t) = S(t) - S^g[T(t)]$ in terms of the instantaneous entropy $S(t)$. The relaxation time varies with cooling below T_g and with annealing time through $S(t)$.

The details of calculation 3 will be explained shortly. Calculation 1 examines which features of enthalpy relaxation are quantitatively accounted for by the calculation in terms of the equilibrium relaxation time $\tau^{eq}(T)$ and to what extent the deviation in τ^{eq} from $\tau(t)$ quantitatively affects the calculation under a given thermal history. Note that in the out-of-equilibrium state the relaxation time is already much longer than the time scale of observation. After discussing the limitation of the description of the out-of-equilibrium state by the equilibrium relaxation time in calculation 1, we take account of the out-of-equilibrium state, or the nonlinearity

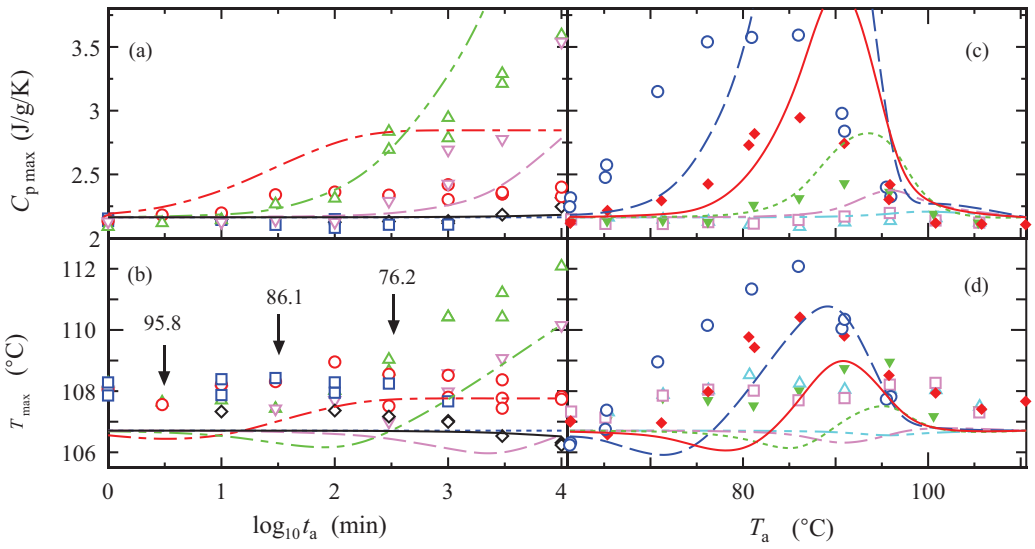

FIG. 10. (Color online) Annealing time dependence of (a) $C_{p\,max}$ and (b) T_{max} at $T_a = 61.3\,^\circ$C (◇), 76.2 °C (▽), 86.1 °C (△), 95.8 °C (○), and 110.6 °C (□). The arrows indicate $t_{amin}(T_a)$. The curves represent the results from calculation 3. The solid, dashed, dash–double-dotted, dash-dotted, and dotted lines are $T_a = 61.3\,^\circ$C, 76.2 °C, 86.1 °C, 95.8 °C, and 110.6 °C, respectively. Also shown is the annealing temperature dependence of (c) $C_{p\,max}$ and (d) T_{max}. The symbols and the line types are the same as in Fig. 7(b).

in the simplest form $S_c(t) = S(t) - S^g[T(t)]$ in calculation 2. In these two calculations the parameters only experimentally obtained are employed. In calculation 3, the better agreement with the experimental results is examined by taking account of the additional contribution of the specific heat to the glassy entropy $S^g(T)$. The relaxation time depends on $S(t)$ in calculations 2 and 3. In these cases, since the right-hand side of Eq. (1) contains $S(t)$ through Eqs. (3)–(5), the numerical calculations of $S(t)$ from the previous time step are repeated until the values of $S(t)$ coincide on both sides of Eq. (1) within the accuracy of the calculation.

The thick cyan (light gray) curves in Figs. 6(b), 8(b), and 9(b) show the specific heat on heating from calculation 1 under the same thermal history as that of the rate cooling and the annealing experiments. The maxima of the specific heat at about 108 °C are reproduced by this calculation and $C_{p\max}$ increases with decreasing $\dot{T}_c$ and increasing t_a, in agreement with the experimental results (ii). However, $T_{\max}$ only decreases with decreasing $\dot{T}_c$ and increasing t_a and calculation 1 does not reproduce the experimental results (iii). In calculation 1, where the relaxation time is assumed to be determined only by temperature through Eq. (4) with $S_c(T) = S^{eq}(T) - S^g(T)$, the annealing time dependence of the specific heat is noticeable at $90.9 \leqslant T_a \leqslant 95.8$ °C. The origin of the result that $C_p(t)$ on heating is independent of t_a at $T_a \leqslant 85$ °C within $t_a \leqslant 10^4$ min is that the relaxation time is too long for the entropy to relax during the annealing time t_a up to 10^4 min: The relaxation time $\tau(T)$ is 7.9×10^8 s at 85 °C, 1.8×10^5 s at 90.9 °C, and 1.7×10^3 s at 95.8 °C, as shown in Fig. 4.

The results of calculation 2, where the configurational entropy is assumed to be determined by the instantaneous entropy by $S_c(t) = S(t) - S^g[T(t)]$, are shown by the blue (dark gray) fine curves in Figs. 6(b), 8(b), and 9(b). Though $C_{p\max}$ increases with t_a in qualitative agreement with the experimental results (ii), the calculated specific heat has a much larger peak at a higher temperature than that of the experimental one. Further, $T_{\max}$ moves toward only higher temperatures with decreasing $\dot{T}_c$ and increasing t_a. These results are considered to be due to the short relaxation time at T_a in the calculation.

The annealing time dependence of the peak temperature in specific heat is discussed on the bases of the results of calculations 1 and 2. As shown in Fig. 1, the cooling process starts at $t = 0$ in equilibrium, the sample is annealed from t_{AN} to t_{CL2}, and the reheating process starts at t_{HT}. The integral in Eq. (1) during the heating process $t > t_{HT}$ is decomposed into two components $\delta S_{ba}(t)$ and $\delta S_{aa}(t)$, the contribution to $\delta S(t)$ before and after annealing, respectively:

$$\delta S(t) = S(t) - S^{eq}[T(t)] = \delta S_{ba}(t) + \delta S_{aa}(t) \tag{9}$$

$$= -\int_0^t \overline{\Delta\chi}[T(t),T(t')][T(t) - T(t')]\frac{\partial\phi[\tilde{t}(t,t')]}{\partial t'}dt', \tag{10}$$

$$\delta S_{ba}(t) = -\int_0^{t_{AN}} \overline{\Delta\chi}[T(t),T(t')][T(t) - T(t')]\frac{\partial\phi[\tilde{t}(t,t')]}{\partial t'}dt' + \overline{\Delta\chi}[T(t),T_a][T(t) - T_a]\phi[\tilde{t}(t,t_{AN})], \tag{11}$$

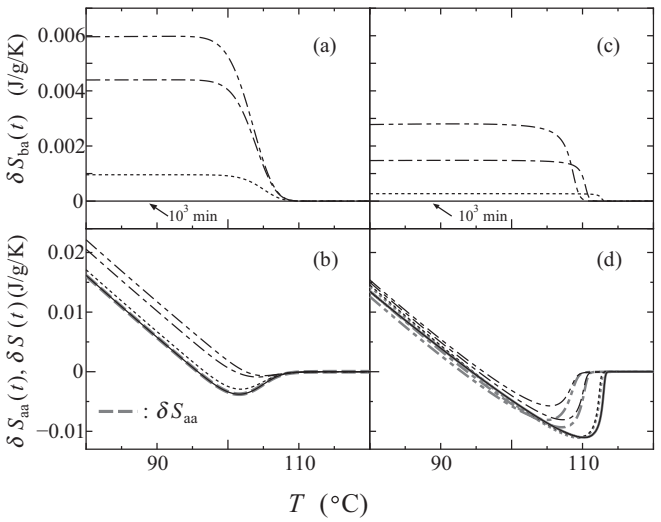

FIG. 11. Variation with annealing time of (a) $\delta S_{ba}(t)$ and (b) $\delta S_{aa}(t)$ (thick) and $\delta S(t)$ from calculation 1 on heating at $T_a = 95.8$ °C and (c) $\delta S_{ba}(t)$ and (d) $\delta S_{aa}(t)$ (thick) and $\delta S(t)$ from calculation 2. The line types are the same as in Fig. 7(b).

$$\delta S_{aa}(t) = -\overline{\Delta\chi}[T(t),T_a][T(t) - T_a]\phi[\tilde{t}(t,t_{CL2})] - \int_{t_{CL2}}^t \Delta\overline{\chi}[T(t),T(t')][T(t) - T(t')]\frac{\partial\phi[\tilde{t}(t,t')]}{\partial t'}dt'. \tag{12}$$

In Eq. (10) the integral during annealing from t_{AN} to t_{CL2} gives $\overline{\Delta\chi}[T(t),T_a]\{\phi[\tilde{t}(t,t_{CL2})] - \phi[\tilde{t}(t,t_{AN})]\}$ since $T(t') = T_a = \text{const}$. This contribution is divided into the second term of the right-hand side of Eq. (11) and the first term of Eq. (12) and included in δS_{ba} and δS_{aa}, respectively.

Figures 11(a) and 11(b) show $\delta S_{ba}(t)$ and $\delta S_{aa}(t)$ in the heating process from calculation 1 at $T_a = 95.8$ °C and t_a from 1 to 10^3 min. Figure 11(a) indicates that $\delta S_{ba}(t)$ decreases with t_a due to the relaxation during annealing. In calculation 1, $\delta S_{aa}(t)$ decreases with T in the glassy state and approaches the equilibrium value at high temperature with an undershoot as shown in Fig. 11(b) by a thick dashed line. The component $\delta S_{aa}(t)$ is common to all the annealing times t_a since the configurational entropy S_c and hence the relaxation time are determined only by temperature and are independent of the thermal history in calculation 1. The deviation in entropy from the equilibrium value during heating $\delta S[T(t)] = \delta S_{ba}[T(t)] + \delta S_{aa}[T(t)]$ for each t_a is also shown in Fig. 11(b). Since the inflection point of $\delta S[T(t)]$ approximately corresponds to $T_{\max}$ in Figs. 8 and 9, Fig. 11(b) indicates that the decrease in the component before annealing $\delta S_{ba}[T(t)]$ leads to the decrease in $T_{\max}$ with increasing annealing time.

In calculation 2, since $S(t)$ is larger than $S^{eq}[T(t)]$ at $T(t) < T_g$, the instantaneous relaxation time $\tau(t)$ is shorter than the equilibrium relaxation time $\tau[S^{eq}(T)]$. Because of the decrease in $S(t)$ during annealing, the relaxation time after annealing ($t > t_{CL2}$) increases toward $\tau^{eq}(T_a)$ with increasing annealing time t_a at a given annealing temperature. Figures 11(c) and 11(d) show $\delta S_{ba}(t)$ and $\delta S_{aa}(t)$ from calculation 2 at $T_a = 95.8$ °C and t_a from 1 to 10^3 min. The variation of $\delta S_{ba}(t)$ with annealing time in calculation 2 is qualitatively similar to that

in calculation 1 [Fig. 11(a)]. Owing to a shorter relaxation time $\tau(t_{AN})$ than in the case of calculation 1, the component δS_{ba} is accordingly smaller due to the faster relaxation in entropy. Since the relaxation time $\tau[T(t)]$ after annealing ($t > t_{CL2}$) becomes longer with increasing t_a, the response of $S(t)$ against the temperature variation is delayed and the temperature at which $\delta S_{aa}(t)$ and the resultant $\delta S(t)$ approach the equilibrium increases with t_a as shown in Fig. 11(d). The aging effect that the relaxation time increases with t_a therefore leads to the increase in T_{max} with t_a. In this way, the annealing has two opposite effects on the variation of T_{max}: The decrease in the component $\delta S_{ba}(t)$ before annealing gives rise to the decrease in T_{max} and the increase in relaxation time during and after annealing gives rise to the increase in T_{max}. The experimental results of aPS (iii) indicate that the simple relaxation in entropy is the main outcome of annealing in the initial stage followed by the increase in relaxation time due to the physical aging and $t_{a\,min}(T_a)$ in Fig. 10(b) is a crossover annealing time between these effects.

Now the correspondence between the TNM model and our calculations is examined. Instead of the TNM model of the Arrhenius type, the Adam-Gibbs theory has been applied to the history dependence of the relaxation time [12]. Hutchinson *et al*. proposed the following configurational entropy dependent on both temperature and fictive temperature [15,17]:

$$S_c(T,T_f') = x_s S_c(T) + (1 - x_s) S_c(T_f'), \tag{13}$$

where x_s is an entropic nonlinearity parameter ($0 \leqslant x_s \leqslant 1$). In calculation 1, the configurational entropy is defined by $S_c(T) = S^{eq}(T) - S^g(T)$, which corresponds to Eq. (13) with $x_s = 1$. In calculation 2, the configurational entropy is defined by $S_c(t) = S(t) - S^g[T(t)]$, which is equivalent to $S_c(T_f) = S^{eq}(T_f) - S^g(T_f)$, which corresponds to Eq. (13) with $x_s = 0$. Since the nonlinearity parameter x_s takes a value between 0 and 1, the TNM model with the Adam-Gibbs-type relaxation time assumes the configurational entropy between $S^{eq}(T) - S^g(T)$ and $S(t) - S^g[T(t)]$.

So far the calculations have been carried out based on the relaxation parameters experimentally obtained and no fitting parameter has been introduced. The introduction of nonlinearity parameters [6–9] and the limiting entropy attained after infinitely long annealing [10,19] are candidates to accommodate the relaxation time to one between the values of τ in calculations 1 and 2. Although calculation 2 qualitatively explains the experimental results, we introduce the following concept for further quantitative discussion. Recently, the relation between configurational entropy and specific heat has been studied based on the free energy landscape theory [22–24]. These studies suggest that the configurational entropy is not given by Eq. (5) and besides $C_p^{\infty}(T)$ the glassy entropy $S^g(T)$ includes an additional contribution of specific heat $\Delta C(T)$ originating from the temperature dependence of the FEL and changes stepwise presumably in the glass transition region.

Calculation 3. Based on the FEL theory, the influence of an additional contribution $\Delta C(T)$, either positive or negative, is examined as calculation 3. The glassy entropy $S^{g\prime}(T)$, which takes account of $\Delta C(T)$, is given by

$$S^{g\prime}(T) = S^{eq}(T_2') + \int_{T_2'}^{T} \frac{C_p^{\infty}(T') + \Delta C(T')}{T'} dT', \tag{14}$$

$$\Delta C(T) = \sqrt{\frac{2}{\pi}} \Delta\chi_F T \exp\left[- \frac{(T - T_F)^2}{2\sigma_F^2} \right], \tag{15}$$

where one of the simplest functional forms to give a stepwise increase in $S^{g\prime}(T)$, as shown in Fig. 2 by the dash-dotted curve, is assumed for $\Delta C(T)$ and $\Delta\chi_F$, σ_F, and T_F are the constant parameters independent of temperature and the experimental condition. The configurational entropy is given by $S_c(t) = S(t) - S^{g\prime}[T(t)]$ and the relaxation time by Eq. (4). The parameters $\Delta\chi_F$, σ_F, and T_F are determined by a trial and error method so that δS (50 °C) at $t_a = 10^4$ min of the calculation agrees with the experimental results as shown in Fig. 7(b) by the solid line; $\Delta\chi_F = -6.17 \times 10^{-4}$ J g^{-1} K^{-2}, $\sigma_F = 23$ K, and $T_F = 371$ K. The least-squares fitting to the experimental relaxation time by Eq. (4) with this set of parameters gives $\tau_\infty^{(3)} = 4.35 \times 10^{-9}$ s, $A^{(3)} = 550$ J g^{-1}, and $T_2^{(3)} = 329$ K and is shown in Fig. 4 by the dotted line.

The results from calculation 3 are shown in Figs. 6–10. The agreement with the experimental results is improved and the results (i)–(iii) are qualitatively reproduced. Figure 7(a) shows the cooling rate dependence of $\delta S(T_{low})$ in calculation 3 together with that in calculations 1 and 2. Though the calculated values of T_{max} are lower than the experimental ones by about 2 K partly due to the uncertainty in reading the peak temperature of C_p'' in Fig. 3, calculation 3 quantitatively reproduces the variation in $C_{p\,max}$ and T_{max} with annealing temperature and annealing time for $t_a \leqslant 10^2$ min [Figs. 8(a), 9(a), and 10(a)] and for cooling rate $T_c \geqslant 1$ K/min [Fig. 6(a)]. For $t_a > 10^2$ min, however, $C_{p\,max}$ in calculation 3 gives larger values and T_{max} gives lower values than the experimental results. The annealing time dependence of the relaxation time and specific heat will be discussed based on the calculation with parameters $\Delta\chi_F$, $\Delta\sigma_F$, and T_F despite the insufficient quantitative agreement at long annealing times.

During annealing, the configurational entropy decreases from $S_c(t_{AN})$ toward $S_c(T_a)$ and accordingly the relaxation time increases from $\tau(t_{AN})$ toward $\tau^{eq}(T_a)$. Figure 12 shows the change in $\delta S(t) = S_c(t) - S_c(T_a)$ and $\tau(t)$ during annealing. Struik pointed out that the relaxation time or the shift factor increases with annealing time to the power of t_a [1]. In fact, the power dependence of $\tau(t_a) = \tau(t - t_{AN})$ on t_a is observed in the long t_a region at $T_a \leqslant$86.1 °C in Fig. 12. The vertical arrows in Fig. 12 show the crossover times $t_{a\,min}(T_a)$; the solid arrows show the experimental results in Fig. 10(b) and the dashed arrows show the calculations. Though the calculations give longer $t_{a\,min}$ than the experimental results, it turns out [Fig. 12(a)] that the aging effect on relaxation time becomes effective when the entropy decays from $\delta S(t_{AN})$ by 20–40%. The time at which $\tau(t)$ during annealing begins to show the power dependence on t_a is similar to $t_{a\,min}$ from calculation 3 in Fig. 10(b). This indicates that T_{max} decreases at shorter t_a where the increase in $\tau(t)$ is small and increases at longer t_a where $\tau(t)$ shows a power-law increase.

Since the relaxation time at the end of annealing $\tau(t_{CL2})$ is longer for longer annealing time at a given T_a, $\delta S(t)$ is smaller and $\tau(t)$ is longer at time t after annealing. Figure 13 shows

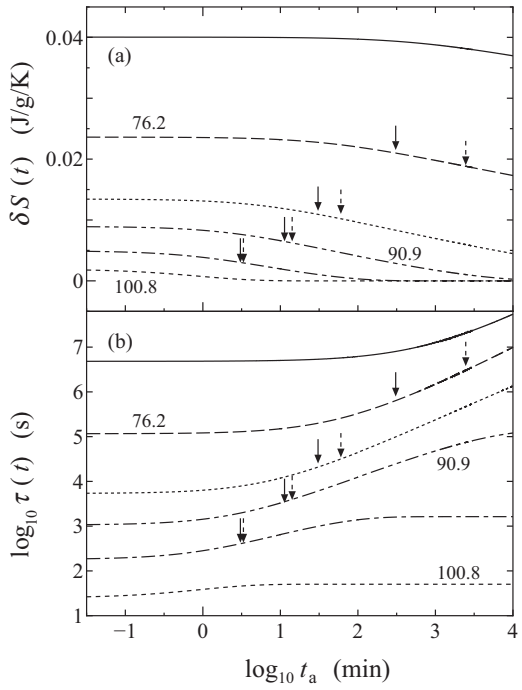

FIG. 12. Change in (a) $\delta S(t)$ and (b) $\tau(t)$ from calculation 3 during annealing. The solid, dashed, dotted, dash–double-dotted, dash-dotted, and short-dashed curves are $T_a = 65.3$ °C, 76.2 °C, 86.1 °C, 90.9 °C, 95.8 °C, and 100.8 °C, respectively. The solid arrows show the experimental $t_{a\,min}$ and the dashed arrows the calculated $t_{a\,min}$. The numbers in the figure represent the annealing temperature.

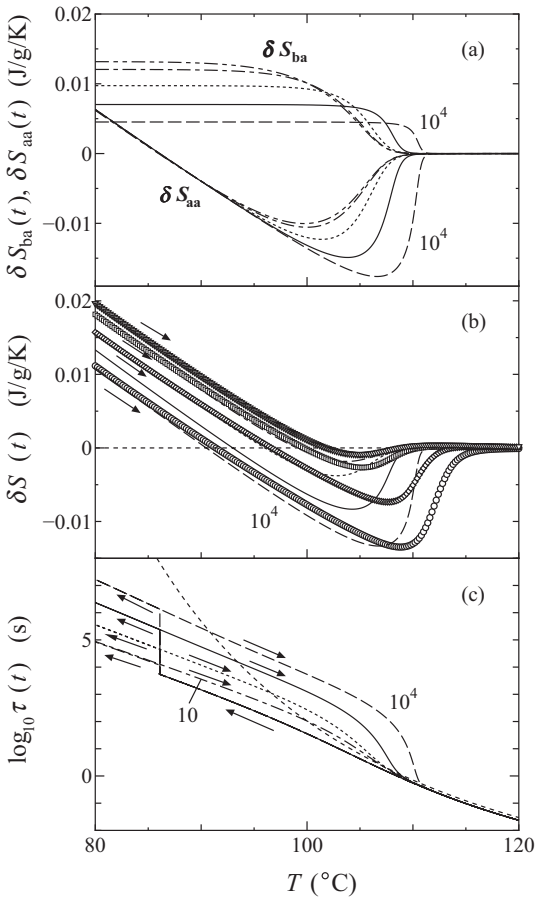

FIG. 13. Temperature dependence of (a) $\delta S_{ba}(t)$ (upper) and $\delta S_{aa}(t)$ (lower), (b) $\delta S(t)$, and (c) $\tau(t)$ on heating at $T_a = 86.1$ °C for t_a in the range from 1 to 10^4 min. (b) Experimental $\delta S(t)$: ▽, $t_a = 10$; □, $t_a = 10^2$; ◇, $t_a = 10^3$; and ○, $t_a = 10^4$ min. The curves represent the results from calculation 3. The calculated $\delta S(t)$ and $\tau(t)$ for $t_a = 1$ min are not shown in the figures. The line types are the same as in Fig. 7(b). The dashed line in (c) represents the temperature dependence of the relaxation time in equilibrium τ^{eq}. The left pointing arrows in (b) and (c) show the cooling process before heating in the annealing experiments. The numbers in the figure represent the annealing time.

the temperature dependence of $\delta S_{ba}(t)$, $\delta S_{aa}(t)$, $\delta S(t)$, and $\tau(t)$ on heating for $T_a = 86.1$ °C. Figure 13(a) shows that at short t_a the decrement in $\delta S_{ba}(t)$ is dominant over the decrement in the minimum of $\delta S_{aa}(t)$ in the change in $\delta S(t)$ with t_a because of the small change in $\tau(t)$ with t_a, which causes the decrease in T_{max} with t_a, while at long t_a the latter is dominant over the former because of the large change in $\tau(t)$, which causes the increases in T_{max}. Thus the interplay between the decrease in δS_{ba} and the increase $\tau(t)$ given rise by annealing results in the change in T_{max} with t_a.

The better agreement with the experimental results than the present study was obtained by the parameter fitting method with models similar to Eq. (1) [10,18,37]. Regarding the origin of the discrepancy between our experimental and calculated results at long annealing time noted above, the following factors are considered: the oversimplified functional form of Eq. (15) assumed for the additional contribution to the specific heat based on the FEL theory, the application of the KWW function to the relaxation function, unnoticed factors determining the relaxation time, and so on. Of these, the long time behavior of the relaxation function may be influential to the enthalpy relaxation under the heavy aging conditions. The power-law decay in the long time region in the relaxation function is observed in the dielectric measurements [38], though not confirmed in the experimental accuracy of the present study. As the slow decay in the long time region would broaden the width of the peak in specific heat on heating and reduce the peak height, better agreement between the experimental and calculated results would be expected. Further, since better agreement at long annealing time has been reported with the introduction of the partitioning parameter x and the configurational entropy of the limit state $S_c^{lim}(T)$, the examination of the physical significance of these quantities, in particular the relationship between $S_c^{lim}(T)$ and $S^{eq}(T) - S^{g\prime}(T)$, is an issue for future research.

V. CONCLUSION

The dependence of enthalpy relaxation on thermal history has been studied by DSC and the phenomenological equation with the thermal relaxation parameters determined experimentally. The contribution of the additional specific heat to the glassy entropy is taken into account based on the FEL theory. The annealing gives rise to the relaxation in entropy arising before annealing and the increase in relaxation time. The crossover of these effects corresponds to the initial decrease and subsequent increase in the peak temperature of specific heat in the heating process after cooling to a temperature well

below T_g. A detail examination of the functional forms of the additional specific heat and the relaxation function in the long time region will be necessary for a thermal history with longer annealing time below T_g and a slower cooling rate.

ACKNOWLEDGMENTS

The authors thank Professor Saruyama of Kyoto Institute of Technology for advice on the DSC measurement and Professor Yoshimori of Kyushu University for helpful discussions.

[1] L. C. E. Struik, *Physical Aging in Amorphous Polymer and other Materials* (Elsevier, Amsterdam, 1978).
[2] K. L. Ngai, *Physical Properties of Polymers*, 3rd ed. (Cambridge University Press, Cambridge, 2004), Chap. 2.
[3] I. M. Hodge, J. Non-Cryst. Solids **169**, 211 (1994).
[4] Y. Miyamoto, K. Fukao, H. Yamao, and K. Sekimoto, Phys. Rev. Lett. **88**, 225504 (2002).
[5] C. T. Moynihan, S. K. Lee, M. Tatsumisago, and T. Minami, Thermochim. Acta **280/281**, 153 (1996).
[6] A. Q. Tool, J. Am. Ceram. Soc. **29**, 240 (1946).
[7] O. S. Narayanaswamy, J. Am. Ceram. Soc. **54**, 491 (1971).
[8] C. T. Moynihan, A. J. Easteal, and M. A. Debolt, J. Am. Ceram. Soc. **59**, 12 (1976).
[9] A. J. Kovacs, J. J. Aklonis, J. M. Hutchinson, and A. R. Ramos, J. Polym. Sci. Phys. Ed. **17**, 1097 (1979).
[10] J. L. Gómez Ribelles and M. Monleón Pradas, Macromolecules **28**, 5867 (1995).
[11] G. Adam and J. H. Gibbs, J. Chem. Phys. **43**, 139 (1965).
[12] I. M. Hodge, Macromolecules **16**, 371 (1983).
[13] I. M. Hodge, Macromolecules **16**, 898 (1983).
[14] I. M. Hodge, Macromolecules **20**, 2897 (1987).
[15] J. M. Hutchinson and M. Ruddy, J. Polym. Sci. Part B-Polymer Physics **26**, 2341 (1988).
[16] J. M. O'Reilly and I. M. Hodge, J. Non-Cryst. Solids **131–133**, 451 (1991).
[17] J. M. Hutchinson, M. D. Ingram, and A. J. Pappin, J. Non-Cryst. Solids **131–133**, 483 (1991).
[18] J. L. Gómez Ribelles, M. Monleón Pradas, A. Vidaurre Garayo, F. Romero Colomer, J. Más Estellésm, and J. M. Meseguer Dueñas, Polymer **38**, 963 (1997).
[19] V. M. Boucher, D. Cangialosi, A. Alegría, and J. Colmenero, Macromolecules **44**, 8333 (2011).
[20] G. Williams and D. C. Watts, Trans. Faraday Soc. **66**, 80 (1970).
[21] W. Sakatsuji, T. Konishi, and Y. Miyamoto, J. Therm. Anal. Calorim. (2013), doi: 10.1007/s10973-012-2908-z.
[22] T. Odagaki, T. Yoshidome, A. Koyama, and A. Yoshimori, J. Non-Cryst. Solids **352**, 4843 (2006).
[23] T. Odagaki and A. Yoshimori, J. Non-Cryst. Solids **355**, 681 (2009).
[24] A. Yoshimori and T. Odagaki, J. Phys. Soc. Jpn. **80**, 064601 (2011).
[25] S. Weyer, A. Hensel, and C. Schick, Thermochim. Acta **304/305**, 267 (1997).
[26] I. M. Hodge, Macromolecules **19**, 936 (1986).
[27] J. M. Hutchinson, S. Montserrat, Y. Calventus, and P. Cortés, J. Non-Cryst. Solids **307–310**, 412 (2002).
[28] J. N. Hay, Polymer **19**, 1224 (1978).
[29] I. W. Gilmour and J. N. Hay, Polymer **18**, 281 (1977).
[30] H. Huth, M. Beiner, S. Weyer, M. Merzlyakov, C. Schick, and E. Donth, Thermochim. Acta **377**, 113 (2001).
[31] S. Weyer, A. Hensel, J. Korus, E. Donth, and C. Schick, Thermochim. Acta **304/305**, 251 (1997).
[32] M. Salmerón, C. Torregrosa, A. Vidaurre, J. M. Meseguer Dueñas, M. Monleón Pradas, and J. L. Gómez Ribelles, Colloid Polym. Sci. **277**, 1033 (1999).
[33] J. M. Hutchinson, S. Smith, B. Horne, and G. M. Gourlay, Macromolecules **32**, 5046 (1999).
[34] J. M. Hutchinson and P. Kumar, Thermochim. Acta **391**, 197 (2002).
[35] V. M. Boucher, D. Cangialosi, A. Alegría, J. Colmenero, I. Pastoriza-Santos, and L. M. Liz-Marzan, Soft Matter **7**, 3607 (2011).
[36] S. L. Simon, J. W. Sobieski, and D. J. Plazek, Polymer **42**, 2555 (2001).
[37] A. Brunacci, J. M. G. Cowie, R. Ferguson, J. L. Gómez Ribelles, and A. Vidaurre Garayo, Macromolecules **29**, 7976 (1996).
[38] K. Fukao and Y. Miyamoto, Polymer **34**, 238 (1993).